Periodic ab Initio Study of the Electronic Structure of α-Al_2O_3 and AlN(w) Surfaces Based on Localized Wannier Functions

Geyser Fernández-Catá†

Instituto Superior de Tecnologías y Ciencias Aplicadas, Av. Salvador Allende y Luaces, La Habana, Cuba

Luis Javier Álvarez

Instituto de Matemáticas, Universidad Autónoma Nacional de México, Av. Universidad 1001, Col. Chamilpa, 62210 Cuernavaca (MOR), México

Roberto Dovesi

Dipartimento IFM, Università di Torino, Via P. Giuria, 7, I-10125 Torino, Italy, and Unitá INFM di Torino, Sezione F, via Giuria 5, I-10125 Torino, Italy

Claudio M. Zicovich-Wilson*

Facultad de Ciencias, Universidad Autónoma del Estado de Morelos, Av. Universidad 1001, Col. Chamilpa, 62210 Cuernavaca (MOR), México

Received: October 20, 2003; In Final Form: March 9, 2004

The behavior of surface undercoordinated Al^{3+} cations as electron acceptors is investigated by means of periodic ab initio calculations. The (0001) surfaces of α-Al_2O_3 and AlN(w) were chosen as representative of the different Al coordination types. The electronic structure was analyzed through the valence localized Wannier functions that allow a straightforward description of the electron pairs in terms of chemical concepts. The relevance of the electron back-donation toward surface Al^{3+} cations in the reconstruction of the surfaces is discussed, and evidence was found that some π-bond character is displayed by the surface Al−X bonds after relaxation. This explains the tendency to form surface Al−X planar layers in this kind of system.

I. Introduction

Aluminum atoms are present in crystalline compounds displaying either 4- or 6-fold coordination. The former is typical of AlX (X = N, P, In) semiconductors (blend or wurtzite structure) and of mixed oxides such as aluminosilicates. Other oxides exhibit 6-fold coordinated Al^{3+} ions (α-alumina, spinels, etc.) or both types of coordination (γ-alumina). Although these are the energetically favored situations, Al atoms with a lower degree of coordination may exist in ionic materials, connected to bulk defects or to surface sites.

As regards compounds with Al in tetrahedral coordination, AlN surfaces have attracted great attention because of the possibility to grow thin films on the basal plane of sapphire or Si-terminated SiC(0001);[1−3] these films show interesting mechanical and optoelectronic properties.[4,5] On the other hand, surfaces obtained from octahedral aluminum oxides, in particular α-Al_2O_3, corundum, are of considerable relevance due to their wide use in semiconductor device technology and as supports in heterogeneous catalysis.[6] Accordingly, several reports have been devoted to the experimental[7−13] and theoretical[14−29] characterization of these systems.

The electronic structure around Al^{3+} cations experiences important changes as the coordination number decreases. From the chemical point of view, whenever coordination is lower than four, these cations may behave as strong electron acceptors and, therefore, display a significant Lewis acidity. Nevertheless, the influence of this behavior on the nature of the bonds in which the undercoordinated Al^{3+} cations are involved is still controversial, in particular concerning surface properties.

In recent theoretical works,[14,15] it was shown that surface reconstruction of Al ended α-Al_2O_3 (0001) surfaces can be, in principle, explained solely in terms of electrostatic and short-range repulsive Pauli forces. It is thus assumed that back-donation from the anions to the three-coordinated Al atom is negligible. On the other hand, other studies[16−19,28] strongly suggest that a certain degree of covalency occurs in the Al−X bonds and that this effect may induce particular structural rearrangements which depend on the Al^{3+} coordination number.

The aim of the present work is to explore to what extent the back-donation toward the undercoordinated Al^{3+} cations is significant for the proper description of the electronic structure of Al containing ionic surfaces. To this purpose, ab initio calculations were performed on periodic 2D models of some selected ionic surfaces that display 3-fold coordinated Al^{3+} cations: the (0001) surfaces of α-Al_2O_3 and AlN(w).

The electronic structure was analyzed through a scheme based on the partition of the valence electronic structure in terms of maximally localized orthogonal Wannier orbitals. Wannier functions (WF), when sufficiently well localized, present many appealing features compared to canonical orbitals, that in periodic calculations have the form of delocalized Bloch functions (BF). In a localized WF basis, the electronic structure of a crystalline compound takes a simple and easy to analyze

* To whom correspondence should be addressed. E-mail: claudio@servm.fc.uaem.mx.

† Instituto de Matemáticas, Universidad Autónoma Nacional de México.

10.1021/jp0371736 CCC: $27.50
Published on Web 04/29/2004

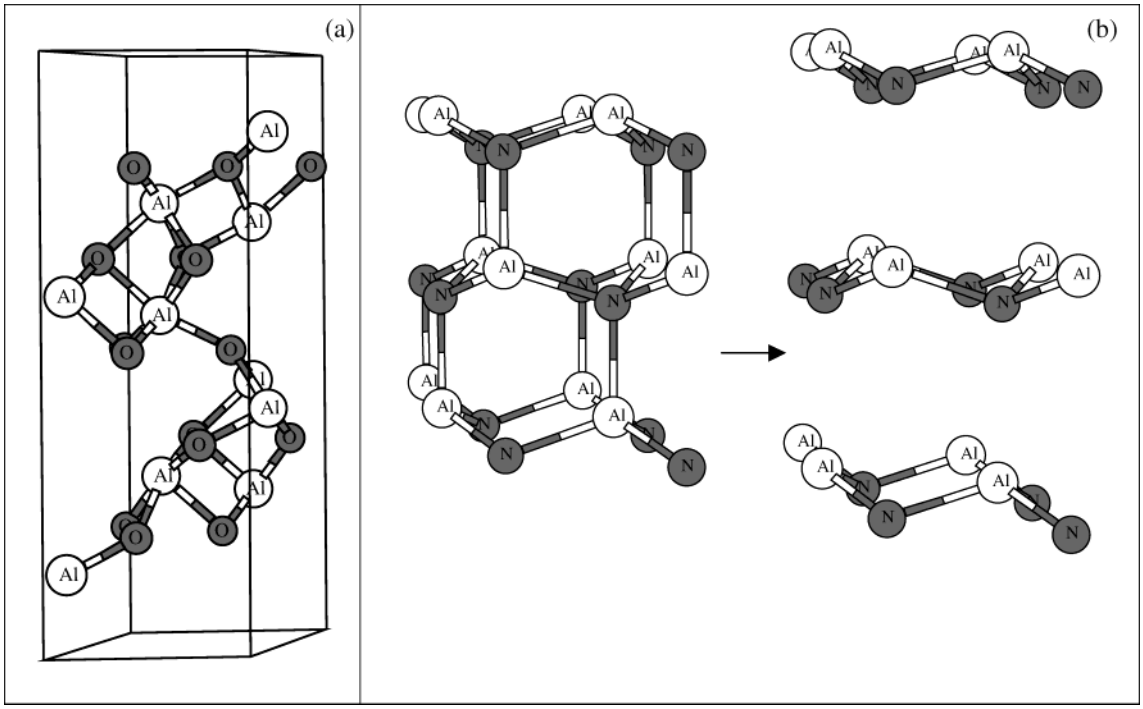

Figure 1. (a) Fifteen layer slab along (0001) surface of Al_2O_3. (b) AlN models.

form to which chemical concepts such as lone pairs, core or valence electrons, and covalent or ionic bonds can be applied not only qualitatively but also quantitatively.[30−33] For closed shell systems, each WF describes a spatially localized state that represents an electron pair in the Lewis picture of chemical bonding. The interpretation is equivalent to that given by other more recent methods such as the topological analysis of the negative of the Laplacian of the electron density[34,35] or of the so-called "electron localization function".[36,37] The main difference between these and the present schemes is the way the partition of the electron density is performed: using topological criteria in the former and defining an orthonormal localized basis set in the latter. The localization scheme for crystalline systems recently implemented[38] in the CRYSTAL03[39] code is here applied to the study of bulk and slab models of the above-mentioned compounds.

II. Computational Details

α-Al_2O_3 has the corundum structure ($R\bar{3}c$) with cell parameters $a = 4.76$ Å and $c = 12.99$ Å.[40] The primitive cell contains 10 atoms, 4 Al and 6 O, with a total of 100 electrons per cell (48 valence). Oxygens are tetrahedrally coordinated, while Al atoms are surrounded by 6 O, featuring two types of bonds with distances 1.855 Å and 1.972 Å.

The most stable form of AlN is wurtzite ($P6_3mc$) with structural parameters: $a = 3.11$ Å, $c = 4.98$ Å, and $u = 0.3821$.[41] The primitive cell has four tetrahedrally coordinated atoms, two Al and two N, with a total of 40 electrons per cell (16 valence). Bonds aligned along the z axis (indicated in the following as Al−N′) are about 0.01 Å larger than the others.

For α-Al_2O_3, the bulk and three different slab models with (0001) Al-ended surfaces were considered. Slabs were chosen to be symmetric with respect to the xy plane, with 15, 9, and 6, layers of atoms, respectively. The 15 slab model is depicted in Figure 1. In all cases, the internal geometrical parameters correspond to the bulk experimental geometry. Surface relaxation have been considered just for models containing 9 layers, optimizing all atomic positions but keeping cell parameters fixed at their crystallographic values.

For AlN, a series of calculations were performed starting from the bulk equilibrium geometry (Al−N′ = 1.9 Å), then increasing this distance to 2.9, 3.9, and 4.9 Å. The remaining bond distances and angles were kept fixed at the experimental values. The way that the different models are constructed is represented in Figure 1. Finally, a calculation on a two layer slab parallel to the (0001) surface was carried out, to represent the fully dissociated structure (Al−N′ = ∞). These models will be referred to as: (1.9), (2.9), (3.9), (4.9), and slab, respectively.

Periodic calculations were performed at the Hartree−Fock level using the CRYSTAL03[41] ab initio program. An all electron basis set was employed for all atoms (84-111G*, 73-11G*, and 84-11G*, for Al, N, and O, respectively).[42,43] Standard conditions as described in the CRYSTAL manual[41] were adopted for the accuracy in the integral evaluation. In all cases, a shrinking factor $S = 6$ was used for sampling in the Brillouin zone in the energy calculation; in the localization step, $S = 12$ was used.

As regards the localization scheme, we refer to a general paper[40] for a complete description of its characteristics and for numerical tests showing the dependence of the degree of localization on the computational parameters. Here we simply outline its most relevant features.

In CRYSTAL, BFs, $\psi_s(\mathbf{k})$, are given in terms of a basis set of atomic orbitals (AOs), $\{\varphi_\mu(\mathbf{r}\text{-}\mathbf{s}_\mu\text{-}\mathbf{g})\}$, as

$$\psi_s(\mathbf{r},\mathbf{k}) = \sum_{\mu=1}^{M} \alpha_\mu s(\mathbf{k}) \sum_{\mathbf{g}} e^{i\mathbf{k}\mathbf{g}} \varphi_\mu(\mathbf{r} - \mathbf{s}_\mu - \mathbf{g}) \qquad (1)$$

where $\mathbf{k}$ is a reciprocal lattice vector within the first Brillouin zone (BZ), and the first and second sums in the rhs run over the AOs in the reference cell and the lattice cells, respectively. Accordingly, provided $\{\psi_s(\mathbf{k}), \forall \mathbf{k} \in \mathrm{BZ}\}$, any of the reference WFs of band s, in the AO basis set, is given by

$$\omega_s(\mathbf{r}) = \sum_{\mu=1}^{M} \sum_{\mathbf{g}} c_\mu s^{\mathbf{g}} \varphi_\mu(\mathbf{r} - \mathbf{s}_\mu - \mathbf{g}) \qquad (2)$$

where the orthonormality condition $\langle \omega_s{}^{\mathbf{g}} | \omega_s{}^{\mathbf{g}'} \rangle = \delta_{\mathbf{g}\mathbf{g}'}$ holds for

the periodic images $|\omega_s{}^{\mathbf{g}}\rangle \equiv \omega_s(\mathbf{r}-\mathbf{g})$, on the s-th reference WF. Coefficients $\alpha_{\mu s}(\mathbf{k})$ and $c_{\mu}s^{\mathbf{g}}$ in eqs 1 and 2, respectively, are related by Fourier-like transforms.

WFs can be characterized in terms of their Mulliken atomic populations, defined as

$$q_{A,s}{}^{\mathbf{g}} = \sum_{\mu\in A}\sum_{\nu,\mathbf{g}'} c_{\mu s}{}^{\mathbf{g}} c_{\nu s}{}^{\mathbf{g}+\mathbf{g}'} S_{\mu\nu}{}^{\mathbf{g}'} \tag{3}$$

where the first sum runs over the AOs μ centered on atom A and the second one over all the AOs ν and cells $\mathbf{g}'$. Typically $q_{A,s}{}^{\mathbf{g}}$ gives the contribution of the electron pair described by WF s to the total population ascribed to atom A in cell $\mathbf{g}$. Accordingly, populations are here normalized to 1

$$\sum_{A,s} q_{A,s}{}^{\mathbf{g}} = 1. \tag{4}$$

Starting from a set of N bands given in terms of BFs $\{\psi_s(\mathbf{k}_j)\}_{s=1}^{N}$ where $j = 1,...,L$, the present method generates a set of localized WFs (LWF) that spans the same subspace as the original BFs. Essentially, the method consists of the iterative application of two interdependent steps: (1) a wannierization step, that provides WFs as similar as possible to a given set of spatially localized model functions and (2) a Boys-like localization, which is performed within the subspace just spanned by a set of reference WFs, given in the form of eq 2.

At the end of each cycle, the overall delocalization index is calculated as

$$\Lambda = \left[\frac{1}{N}\sum_{s=1}^{N}\sum_{A,\mathbf{g}} (q_{A,s}{}^{\mathbf{g}})^2\right]^{-1} \tag{5}$$

and the iterative process stops when the absolute difference in Λ between two consecutive cycles is less than a given threshold. In practice, several techniques, detailed elsewhere,[40] are implemented so as to improve the performance of the method. Finally, the localization degree of the previous LWFs is improved by using a Boys-like localization procedure suitable for periodic systems.[44]

Only valence states have been considered for localizing all systems. LWFs are analyzed in terms of both graphical representations and a set of indices that permit a quantitative characterization. They are the following:

(1) The Mulliken atomic populations, $q_{A,s}{}^{\mathbf{g}}$, of atom A in cell $\mathbf{g}$ for the s-th WF, defined in eq 3. Given atom A in the reference cell, the gross Mulliken atomic charge on it for the whole electron density will be expressed as

$$Q_A = Z_A - 2\sum_{\mathbf{g},s} q_{A,s}{}^{\mathbf{g}},$$

where Z_A is the nuclear charge of A, and the sum is performed over all WFs s and lattice vectors $\mathbf{g}$.

(2) The atomic delocalization index of WF s, λ_s, that reads

$$\lambda_s = [\sum_{A,\mathbf{g}} (q_{A,s}{}^{\mathbf{g}})^2]^{-1}. \tag{6}$$

This quantity is nothing else than the inverse participation ratio of the Mulliken atomic populations of WF s and can be considered as a measure of the extent of the electron pair density in terms of the number of "contributing" atoms.[45] Let us consider an example. Suppose, for instance, that, for the sake of illustration, we consider two limiting cases. In the first one, the electron pair density given by WF s is equally distributed along N atoms. Therefore, each atomic population, $q_{A,s}{}^{\mathbf{g}}$, would be equal to $1/N$ and, through eq 6, $\lambda = N$ giving exactly the number of atoms along which the corresponding electron-pair density is delocalized. In the other case, the electron pair density is localized on only one atom, and accordingly, there is only one term equal to 1 in the sum of eq 6 giving, as expected, $\lambda = 1$. The overall delocalization index Λ given in eq 5 is just the geometric average of the λ_s.

(3) The centroid position, $\mathbf{o}_s$, defined by

$$\mathbf{o}_s = \int d\mathbf{r}|\omega_s(\mathbf{r})|^2\mathbf{r} \tag{7}$$

(4) Indices derived from the second-order central moment tensor, $T_{s,lm}$, of the electron density associated to WF s. This tensor is given by

$$T_{s,lm} = \int d\mathbf{r}|\omega(\mathbf{r})|^2(r_l - o_{s,l})(r_m - o_{s,m}) \tag{8}$$

where $\mathbf{r} = (r_1,r_2,r_3)$ and $\mathbf{o}_s = (o_{s,1},o_{s,2},o_{s,3})$. Tensor $T_{s,lm}$ contains useful information on the shape and spatial extent of the electron pair distribution. This information is exploited through the following indices:

(a) The spatial spread, σ_s, which is the square root of the trace of $T_{s,lm}$

$$\sigma_s = (\sum_m T_{s,lm})^{1/2} \tag{9}$$

and the total spatial spread, Ω, which reads

$$\Omega = \sum_s \sigma_s{}^2 \tag{10}$$

These indices are a measure of the mean isotropic spread of the electron pair distributions.

(b) The eigenvalues $A_s \geq B_s \geq C_s$ and their corresponding eigenvectors (i.e., the principal axes of the $|\omega_s(\mathbf{r})|^2$distribution). The eigenvalues contain additional information on the anisotropy of the electron pair density by explicitly considering the spread along the three principal axes.

(c) The uniaxiality, u_s, which is calculated from these eigenvalues through

$$u_s = \frac{A_s - 0.5(B_s + C_s)}{\sigma_s{}^2} \tag{11}$$

This parameter gives a measure of the degree of stretching along the first principal axis of the distribution. It summarizes in any way the information given by the eigenvalues.

(5) The polarization fraction

$$p_s = \frac{2(\mathbf{o}_s - \mathbf{r}_s{}^{q_2})(\mathbf{r}_s{}^{q_1} - \mathbf{r}_s{}^{q_2})}{|\mathbf{r}_s{}^{q_1} - \mathbf{r}_s{}^{q_2}|^2} - 1 \tag{12}$$

where $\mathbf{o}_s$, $\mathbf{r}_s{}^{q_1}$, and $\mathbf{r}_s{}^{q_2}$ are the positions of the centroid and the two atoms with the largest Mulliken populations, respectively. Geometrically, it gives position of the projection of the centroid-nucleus vector along the bond axis, relative to the middle point and normalized by a half of the bond length. The two limiting cases $p = 0$ and $p = 1$ correspond to pure covalent bonds and lone pairs, respectively, as, in the former, the projection of the centroid onto the bond direction is just in the middle of the bond, while, in the latter, it coincides with the position of the most populated atom. This index gives, therefore, a good

measure of the intuitive concept of bond ionicity widely used in chemistry.

For a more detailed discussion on the connection between these indices and the chemical nature of the electron pairs described by the LWFs, we refer to previous works,[31,32] where the present indices have been calculated for series of compounds ranging from full ionic to full covalent bonding character.

III. Results and Discussion

Let us begin our analysis with the unreconstructed surfaces; we shall move then to the reconstructed situation. In the case of corundum models, the LWFs, when classified according to their spatial localization indices, can be attributed in all cases to six different types that are associated to the relative position of the central O atoms with respect to the surface. At first we can distinguish two types: inner (in) and surface (surf), according to whether the O atom to which they belong is surrounded by four Al atoms. The inner LWFs split into two groups, corresponding to the short and long Al−O bonds in bulk (in-s and in-l, respectively); they are also present in the 9 and 15 layer slabs. As regards surface LWFs, the local symmetry breaking at the second layer O atoms gives rise to four different situations: each of the short (s) and long (l) Al−O bond types in the bulk splits into two different sets at the surface, namely surf-s1 and surf-s2, on one hand, and surf-l and surf-lp, on the other hand. surf-l, surf-s1, and surf-s2 correspond to bonds connecting O atoms at the second layer to Al atoms at the fourth, third, and first layers, respectively, whereas surf-lp is a nonbonding lone pair arising from an Al vacancy around the surface O atom. The present notation has been chosen to reflect the relation between the LWFs and the electron pairs in the Lewis picture of chemical bonding.

LWFs belonging to each type slightly differ from each other in the same model and from model to model, but the standard deviation for the various indices discussed below corresponding to LWFs that belong to the same type is always quite small, i.e. < 0.1%.

The average localization indices for each type are given in Table 1. For the sake of comparison, the gross atomic Mulliken populations are also listed in Table 2. In general, the LWFs display similar characteristics as far as their localization properties are concerned. Considering the three largest Mulliken atomic contribution to each LWF, ($q_{A,s}^{g}$, where A corresponds to the central O and two neighboring Al atoms, and $\mathbf{g} = 0$), which are also documented in Table 1, it arises that the most populated atoms for each electron pair distribution are O atoms having more than 90% of the electron density. In addition, λ values close to 1, which measure the extent of the distribution in terms of atomic contributions (see discussion in section II), do indicate that the electron density is mainly localized in the neighborhoods of a single atom. These results support the ionic interpretation of the electronic structure of corundum.

Despite the general high degree of ionicity (see for instance the p_s values listed in Table 1 and their interpretation given in section II), important changes in the electron distribution are observed in going from the inner to the outer LWFs in the various surface models. In Figure 2, the dependence of the delocalization index, λ, on the distance of the centroid to the surface is represented. It turns out that the difference between short and long Al−O bonds decreases monotonically in moving down from the surface to the bulk, attaining fast convergence. The most important changes between bulk and surface situations are experimented by surf-s2 and surf-lp, that must be compared to in-s and in-l, respectively. As it appears from the localization indices given in Table 1, the former undergoes a significant delocalization in going from the bulk to the surface (in-s → surf-s2), while for the latter (in-l → surf-lp) the converse process is observed. This is also reflected in the graphical representation (see the density maps in Figure 3) at least at the qualitative level; in particular it arises that in surf-s2 the electron clouds surround more efficiently the Al atom than in in-s. On the other hand, the density maps apparently shows the lone-pair character of surf-lp.

The larger localization of surf-lp is to be associated to its nonbonding character that gives rise to an electron distribution close to 100% around the O atom.

TABLE 1: Average LocalizAtion Indices and Bond Distances for Oxygen LWFs in Unrelaxed (Unrel) and Relaxed (Rel) (0001) α-Al_2O_3 Surfaces[a]

O-WFs	in-s	in-l	surf-s1	surf-s2	surf-l	surf-lp
			Unrel			
λ_s	1.084	1.048	1.081	1.188	1.040	1.019
σ_s	0.749	0.758	0.753	0.797	0.771	0.776
p_s	0.606	0.644	0.609	0.524	0.686	
u_s	0.192	0.199	0.188	0.224	0.195	0.208
$q^0_{O,s}$	0.960	0.976	0.961	0.914	0.980	0.991
$q^0_{Al(1),s}$	0.043	0.033	0.041	0.084	0.025	0.007
$q^0_{Al(2),s}$	0.002	−0.004	0.006	0.002	0.009	−0.005
δ_s	0.090	0.087	0.107	0.070	0.141	
d[OAl]	1.855	1.972	1.855	1.855	1.972	
			Rel			
λ_s	1.060	1.039	1.098	1.157	1.079	1.037
σ_s	0.755	0.768	0.739	0.741	0.748	0.767
p_s	0.634	0.652	0.589	0.542	0.608	
u_s	0.188	0.205	0.188	0.187	0.192	0.186
$q^0_{O,s}$	0.971	0.981	0.953	0.927	0.962	0.982
$q^0_{Al(1),s}$	0.034	0.029	0.047	0.071	0.041	0.011
$q^0_{Al(2),s}$	0.002	−0.005	0.006	0.003	0.006	0.003
δ_s	0.115	0.095	0.042	0.049	0.036	
d[OAl]	1.937	1.967	1.786	1.674	1.860	

[a] There are six types of O-WFs (see the text for label meaning). For each LWF, we report the following: atomic delocalization index λ_s (in $|e|^{-2}$) (see eq 6); spatial spread, σ_s (in Å) (see eq 9); uniaxiality, u_s (see eq 11); polarization fraction, p_s (see eq 12); the three largest, in absolute value, Mulliken atomic populations of LWF s (see eq 3), $q^0_{O,s}$, $q^0_{Al(1),s}$, and $q^0_{Al(2),s}$ (in $|e|$); and, finally, the offset of the centroid with respect to the O−Al bond line, δ, and the Al−O bond distance, d[OAl] (in Å).

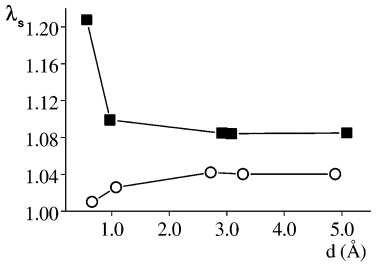

Figure 2. Atomic delocalization index l_s (in $|e|^{-2}$) (see eq 6) for WFs as a function of the distance of the centroid to the surface in the fifteen layer slab. Solid squares and open circles refer to the short and long bonds, respectively (see details in text).

TABLE 2: Gross Mulliken Atomic Charges for the Unrelaxed and Relaxed Al_2O_3 Slabs

layer	atom	unrel	rel
1	Al	2.372	2.433
2	O	−1.639	−1.603
3	Al	2.507	2.479
4	Al	2.518	2.503
5	O	−1.653	−1.737

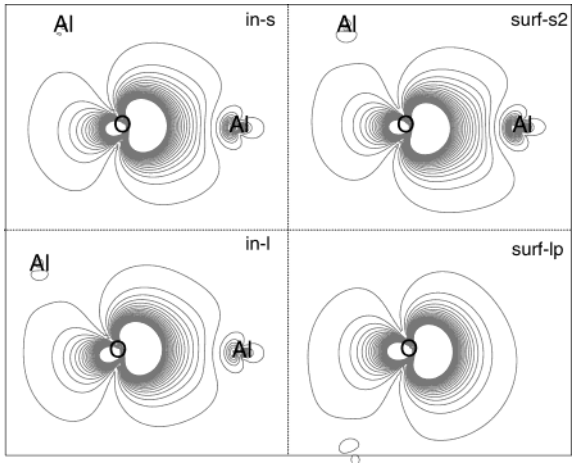

Figure 3. Electron density of in-s, in-l, surf-s2, and surf-lp WFs. The map plane contains two Al and the central O atoms, except for the case of surf-lp where one of the Al atoms is substituted by the centroid position. Isodensities are in the interval [0.001,0.1] |e|/bohr^3 separated by 0.005 |e|/bohr^3.

In a more thorough comparison between surf-s2 and in-s, all indices (see Table 1) suggest that the surface Al−O bond envisages a larger covalent character with respect to the bulk. The larger delocalization with respect to the other LWFs is clearly reflected by the λ and σ values that represent the mean number of atoms involved in the bond and the spatial spread of its electron density, respectively. The large decrease of p indicates a less polarized character of the bond, which is intimately related to the increase of the Mulliken population of Al ($q^0_{Al(1),s}$ in the table) and the concomitant decrease of the O charge. Finally, the uniaxiality, u, indicates an elongation along the bond axis with respect to the corresponding inner bond. The behavior is not likely to be attributed to an electrostatic polarization effect. This is because, at the unrelaxed surface, formation without relaxation will not substantially increase the electrostatic interaction between the O electrons and the neighboring Al cation. This supports the idea that not electrostatic but electronic effects, i.e., the increase of the covalent character, are mainly involved in the process. The increase in covalency displayed in going from in-s to surf-s2 can be estimated in about 8.2%, using the bond polarization index, p_s, as a suitable (and fairly intuitive) measure of the ionic−covalent character of a bond.[31,32] To give an idea of the order of magnitude for the importance of changes involved, previous calculations[31] of the polarization index on a series of oxides along the second raw elements can be considered. It arises that the covalent character of the Al−O bond in surf-s2 is comparable to that of the Si−O bond in α-quartz bulk, as the polarization indices, p_s, are equal to 0.524 and 0.511, respectively, in contrast to the value taken in Corundum bulk, 0.606 (see Table 1). This means that the Al atom fairly behaves in surf-s2 as the next more electronegative element in the Periodic Table.

The larger covalent character of the surface Al−O bonds are not only to be attributed to changes on the O atom alone but also to the undercoordination of the Al atom at the first surface layer. In other words, this three-coordinated Al atom acts as a Lewis acid, because of its charge deficiency, hence increasing the strength of the Al−O bonds to which it is involved. This effect provides a key for a more accurate description of the surface reconstruction processes than the purely ionic approach proposed and used by other authors.[14,15] The idea that this electronic reordering is mainly due to the particular properties of the surface three-coordinated Al atoms is supported by the fact that just the electrons of the surface oxygen atoms are actually affected. On the contrary, the electronic structure of O atoms at the inner layers, fully surrounded by 6-fold coordinated Al, remains essentially identical to the bulk, irrespective of the distance from the surface.

Let us now consider the effect of relaxation. An apparent reorganization of the electron distribution occurs as a result of the concomitant changes in the Al−O bond distances. The bulk and optimized bond distances together with the localization indices of the corresponding LWFs are given in Table 1. It turns out that the changes are particularly evident for the surface electrons, while the small electronic reorganization in the inner layers is probably a consequence of the geometry distortions necessary to compensate the significant surface relaxation.

In terms of the localization properties of the LWFs, the surface reconstruction implies a decrease of the differences between surf-s2 and the other surface bonds, with respect to the unrelaxed system. Apart from the general reduction of σ_s, to be attributed mainly to the general shortening of the Al−O bond lengths, this behavior is apparently displayed by the indices that closely depend on the covalent nature of the electron pairs (i.e., λ_s and p_s). Along this line, while surf-s2 slightly decreases its covalent character as a consequence of relaxation, the other three surface LWFs go in the opposite direction, as it turns out from the corresponding values of λ_s, p_s, $q^0_{O,s}$ and $q^0_{Al(1),s}$, i.e., the populations on the O and the neighboring Al. Particularly interesting is the case of surf-lp, which, in the unrelaxed surface, displays a clear nonbonding character, while, after reconstruction, it features a certain degree of delocalization toward the first layer Al atom, i.e., the one involved in surf-s2.

In agreement with previous results,[15,16] relaxation brings the top atoms down in the O plane at the surface. Therefore, while surf-s2 involves sp atomic orbitals oriented parallel to the surface, surf-lp is directed perpendicular to it, featuring a slight π-bond character with the first Al layer. This is also supported by the uniaxiality, u_s, that decreases under reconstruction. The resulting double bond may be responsible for the more significant shortening of the surface Al−O distance with respect to the other ones. This is in partial agreement with previous findings[16] where an increase in covalent character of the Al−O bond has been reported at the corundum surface, as result from the Mulliken analysis.

Another interesting point is that surface reconstruction gives rise to a general decrease of the offset of the surface LWF centroids, eq 7, with respect to the bond axes, δ_s in Table 1. In other words, after relaxation, the electron pairs are more efficiently polarized toward the Al atoms. It has been shown in a previous work[31] that the bond directionality of the LWFs is to be interpreted as a sign of covalent character, supporting the relevance of these effects in the whole reconstruction process.

A different situation in which large changes in the electronic structure are originated by the undercoordination of Al ions in ionic crystals is given by the formation of AlN films. In this material, just two different types of LWFs occur that correspond to the two different Al−N bonds in the wurtzite structure. The LWF directed along the z axis and connecting atoms in different slabs has multiplicity two, while the other type involves just atoms in the two layer slab, as shown in Figure 1, and displays multiplicity 6. In Table 3, the three highest atomic populations of these LWFs for the different AlN models are listed. As in the case of corundum, the population analysis supports the very ionic description of the system, with most of the electrons associated to the N^{3-} anions. However, an analysis of the

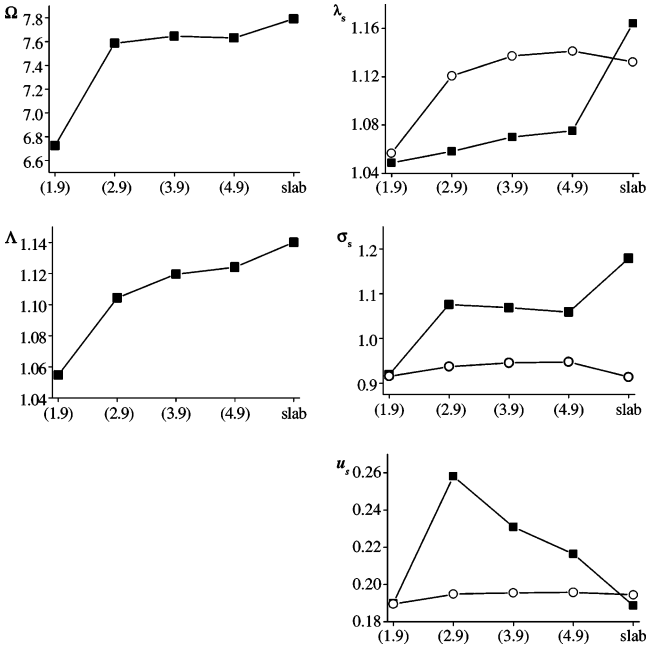

Figure 4. Total spatial spread, W (in Å^2)(see eq 10), and overall delocalization index, L (in $|e|^{-2}$)(see eq 4), for AlN systems. Index of AlN WFs. Atomic delocalization index l_s (in $|e|^{-2}$)(see eq 6), spatial spread, s_s (in Å)(see eq 9), and uniaxiality, u_s (see eq 11). The solid squares refer to the Al−N′ bond, and the open circles refer to the other three bonds (see details in text).

changes along the series of models shows that the general trend is to decrease the ionicity as the Al−N′ distance increases toward infinity (see Figure 1).

The same general trend is also reflected in the evolution of the localization indices shown in Figure 4. The global indices Λ, eq 4, and Ω, eq 10, indicate that the electronic structure features a general delocalization during surface formation. The process can be analyzed in more detail if considering the changes displayed by each type of LWF. Three stages can be identified in the overall process. An initial stage occurs when the Al−N′ distance increases from equilibrium to 2.9 Å. Both types of LWFs present an increase of their delocalized character,

TABLE 3: Mulliken Atomic Populations of the WFs in AlN[a]

r(AlN)	N_{eq}	$q^0_{N,s}$	$q^0_{Al(1),s}$	$q^0_{Al(2),s}$	Q_N	Q_{Al}
1.9	1	0.9754	0.0449	0.0032 (3)	−1.560	2.560
	3	0.9715	0.0479	0.0033 (2)		
2.9	1	0.9719	0.0088	0.0075 (3)	−1.504	2.504
	3	0.9423	0.0651	0.0041 (2)		
3.9	1	0.9665	0.0005	0.0114 (3)	−1.463	2.463
	3	0.9351	0.0701	0.0045 (2)		
4.9	1	0.9639		0.0127 (3)	−1.446	2.446
	3	0.9333	0.0716	0.0047 (2)		
∞	1	0.9257		0.0250 (3)	−1.398	2.398
	3	0.9376	0.0632	0.0066 (2)		

[a] r(AlN) is the Al−N′ distance (in Å); N_{eq} is the number of equivalent nitrogen-WFs; $q^0_{N,s}$, $q^0_{Al(1),s}$, and $q^0_{Al(2),s}$ (in |e|) are the Mulliken atomic populations (see eq 3) of nitrogen, the aluminum atom participating in the bond, and the others aluminum atoms, respectively (the number of equivalent contributions is given in brackets). Q_A refers to the gross atomic charge on atom A.

reflected in the increase of λ and σ, and the concomitant elongation of the electron distribution along the bond axis, reflected in the increase of the uniaxiality, u. During this stage, both types of bonds see their covalent character enhanced as Al−N′ dissociates. In the second stage, occurring at Al−N′ distances between 2.9 and 4.9 Å, only slight changes occur in the indices, except for the case of the uniaxiality of the Al−N′ bond, that decreases toward the value at the equilibrium position. Finally, for Al−N′ distances larger than 4.9 Å, the delocalized character of the Al−N′ bond substantially increases (together with a decrease of the uniaxiality), whereas the other LWF undergoes a slight localization.

This evolution is to be interpreted in terms of both electronic and electrostatic effects. In the first stage, the Al−N′ bond breaking generates an electron deficiency in the Al atom that gives rise to an increase of back-donation from the N atoms and, therefore, to an enhancement of the covalent character of the remaining Al−N bonds. On the other hand, at a not too large Al−N′ distance, the strong electrostatic field created by the array of two layer slabs results in a strong polarization along the z axis, mainly affecting the Al−N′ LWF. After these dramatic changes, the effect of the mutual electrostatic interaction along the z axis decreases. Accordingly, the uniaxiality, u,

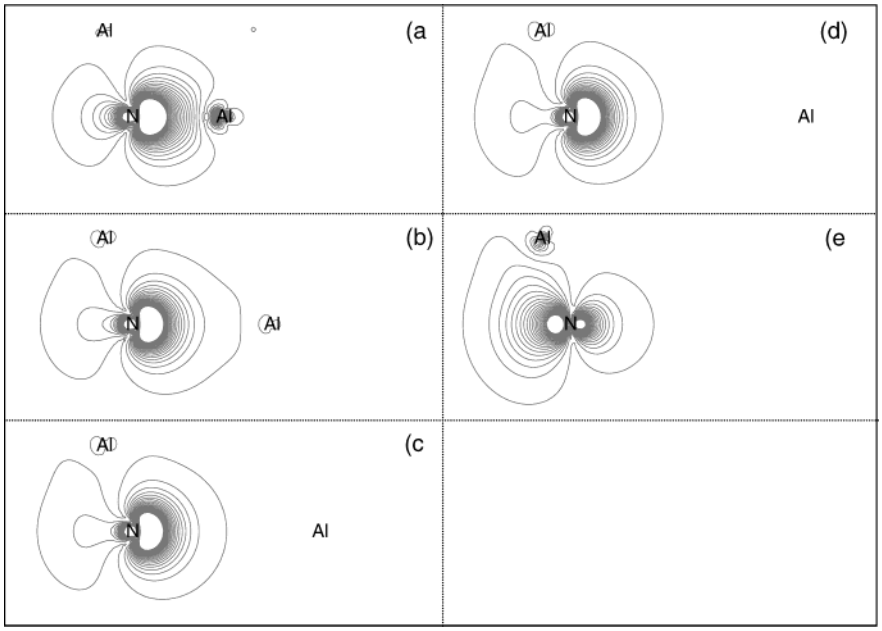

Figure 5. Electron density maps along the plane defined by the three most populated atoms for AlN systems (see Table 3). Labels a−e correspond to interlayer distances (in Å) 1.9, 2.9, 3.9, 4.9, and ∞, respectively. Isodensities are in the interval [0.001,0.1] |e|/bohr^3 separated by 0.005 |e|/bohr^3.

also decreases and a slight delocalization toward Al atoms in the same slab is experimented by the Al−N′ LWF, which is mainly reflected in the increase of λ, while the simultaneous decrease of σ is due to the spatial contraction along the *z* axis. In the last stage, the polarization vanishes at infinite slab separation. This allows the electrons in the lone-pair LWF to delocalize over the slab so as to compensate the electron deficiency of the Al atoms.

This change in the character of the Al−N′ LWF from the bonding toward the lone-pair situations is well illustrated in Figure 5, where the corresponding electron density maps are depicted. It is apparent that, as the strength of the electrostatic field decreases along the *z* direction, due to the increase of the interslab separation, the polarized character of the LWF decreases, yielding to an inversion of the dipole moment vector at the limit of infinite distance. The slight concomitant contraction of the intraslab LWFs may be a consequence of the orthogonality conditions imposed in the calculation.

It is interesting to point out that the delocalization of the dissociated bond in the slab model involves mainly Al p_z orbitals at the neighbors of the N atom, which suggests that a certain degree of π bonding character could be present. This is in close agreement with the results obtained in this work for the reconstruction of the (0001) surface of α-Al_2O_3 and with previous suggestions.[28] According to the case of corundum reconstruction, the planar geometry should be expected to be the most stable for the AlN slab, in the hypothesis of an aromatic-like π delocalization suggested by the fact that the two-layer AlN slab is isoelectronic with graphite. This issue has been verified by performing a full optimization of the AlN two layer slab which, as expected, acquires a hexagonal planar configuration (graphite) with a cell parameter of 3.093 Å.

Summary

The analysis of the electronic structure of α-Al_2O_3 and AlN-(w) by means of their LWFs gives strong evidence that, despite the high ionic nature of the compounds, charge-transfer processes are not negligible in an accurate description of the physicochemical properties of their surfaces. The undercoordinated Al^{3+} ions at surfaces have much more acceptor character than bulk ions, giving rise to a general enhancement of the covalent character of the remaining bonds. The back-donation from the anions toward the Al^{3+} cations can also involve new bonds of π character, whenever the p orbital overlap is allowed by the local geometry relaxation. The present calculations have been performed at Hartree−Fock level, which, as it is well-known, tends to overestimate the ionic nature of the bonds. It is expected that the inclusion of electron correlation effects, for instance, by means of DFT techniques, will give rise to a general enhancement of the covalent interactions in the present case. Therefore, the main conclusion of this work concerning the importance of the covalent interactions in surfaces containing undercoordinated Al^{3+} cations will remain essentially the same.

Acknowledgment. CZW acknowledges support from SEP-FOMES2000 through Project "Cómputo Científico" for unlimited CPU time on the IBM-p690 32-processor supercomputer at UAEM. G.F.C. gratefully acknowledges financial support from Dirección General de Intercambio Académico, UNAM. Calculations of this work were carried out on the IBM supercomputer granted to Instituto de Matemáticas, Unidad Cuernavaca by Fundación Clínica Médica Sur, A. C., and the National Council of Science and Technology (Conacyt) Mexico.

References and Notes

(1) Rouviere, J. L.; Arlery, M.; Bourret, A.; Niebuhr, R.; Bachem, K. H. In *Gallium Nitride and Related Materials*; Dupuis, R. D., Edmond, J. A., Ponce, F. A., Nakamura, S., Eds.; MRS Symposia Proceedings No. 395; Materials Research Society: Pittsburgh, PA, 1996.

(2) Ponce, F. A.; Van de Walle, C. G.; Northrup, J. E. *Phys. Rev. B* **1996**, *53*, 7473.

(3) Strite, S. In *Festkörperprobleme/Advances in Solid State Physics*; Helbig, R., Ed.; Vieweg, Braunschweig, 1995; Vol. 34, p 79.

(4) Nakamura, S.; Senoh, M.; Mukai, T. *J. Appl. Phys.* **1991**, *30*, L1708.

(5) Nakamura, S.; Senoh, M.; Nagahama, S.; Iwasa, N.; Yamada, T.; Matsushita, T.; Kiyoku, H.; Sugimoto, Y. *Jpn. J. Appl. Phys.* **1996**, *35*, L74.

(6) French R. H.; Heuer, A. H. *J. Am. Ceram. Soc.* **1994**, *77*, 292.

(7) Baraton, M. I.; Chen, X.; Gonsalves, K. E. *J. Mater. Chem.* **1996**, *6*, 1407.

(8) Loretz, J. C.; Despax, B.; Martí, P.; Mazel, A. *Thin Solid Films* **1995**, *265*, 15.

(9) Wang, X. D.; Hipps, K. A.; Mazur, U. *Langmuir* **1992**, *8*, 1347.

(10) Mazur, U. *Langmuir* **1990**, *6*, 1331.

(11) Toofan, J.; Watson, P. R. *Surf. Sci.* **1998**, *401*, 162.

(12) Gautier, M.; Renaud, G.; Pham Van, L.; Billete, B.; Pollak, M.; Thromat, N.; Jollet, F.; Duraud, J. P. *J. Am. Ceram. Soc.* **1994**, *77*.

(13) Ahn, J.; Rabalais, J. W. *Surf. Sci.* **1997**, *388*, 121.

(14) Gomes, J. R. B.; Moreira, I. de P. R.; Reinhart, P.; Wander, A.; Searle, B. G.; Harrison, N. M.; Illas, F. *Chem. Phys. Lett.* **2001**, *341*, 412.

(15) Baxter, R.; Reinhardt, P.; López, N.; Illas, F. *Surf. Sci.* **2000**, *445*, 448.

(16) Puchin, V. E.; Gale, J. D.; Shluger, A. L.; Kotomin, E. A.; Günster, J.; Brause, M.; Kempter, V. *Surf. Sci.* **1997**, *370*, 190.

(17) Salasco, L.; Dovesi, R.; Orlando, R.; Causà, M.; Saunders, V. R. *Mol. Phys.* **1991**, *72*, 267.

(18) Causà, M.; Dovesi, R.; Pisani, C.; Roetti, C. *Surf. Sci.* **1989**, *215*, 259.

(19) Pisani, C.; Causà, M.; Dovesi, R.; Roetti, C. *Prog. Surf. Sci.* **1987**, *25*, 119.

(20) Verdozzi, C.; Jennison, D. R.; Schultz, P. A.; Sears, M. P. *Phys. Rev. Lett.* **1999**, *82*, 799.

(21) Wang, X. G.; Chaka, A.; Scheffler, M. *Phys. Rev. Lett.* **2000**, *84*, 3650.

(22) Manassidis, I.; De Vita, A.; Gillan, M. J. *Surf. Sci.* **1993**, *285*, L517.

(23) Manassidis, I.; Gillan, M. J. *J. Am. Ceram. Soc.* **1994**, *77*, 335.

(24) Kruse, C.; Finnis, M. W.; Milman, V. Y.; Payne, M. C.; De Vita, A.; Gillan, M. J. *J. Am. Ceram. Soc.* **1994**, *77*, 431.

(25) Godin, T. J.; LaFemina, J. P. *Phys. Rev. B*, **1994**, *49*, 7691.

(26) Grossner, U.; Furthmüller, L.; Bechstedt, F. *Phys. Status Solidi* **1999**, *216*, 675.

(27) Fritsch, J.; Sankey, O. F.; Schmidt, K. E.; Page, J. B. *Phys. Rev. B* **1997**, *55*, 15360.

(28) Pandey, R.; Zapol, P.; Causà, M. *Phys. Rev. B* **1987**, *55*, R16009.

(29) Northrup, J. E.; Di Felice, R.; Neugebauer, *J. Phys. Rev. B* **1997**, *55*, 13878.

(30) Bert, A.; Llunell, M.; Dovesi, R.; Zicovich-Wilson, C. M. *Phys. Chem. Chem. Phys.* **2003**, *5*, 5319.

(31) Julg, A. *Int. J. Quantum Chem.* **1984**, *26*, 709.

(32) Pipek, J.; Varga, I. *Phys. Rev. A* **1992**, *46*, 3148.

(33) Calzado, C. J.; Malrieu, J.-P.; Sanz, J. F. *J. Phys. Chem. A* **1998**, *102*, 3659.

(34) Bader, R. F. W. *Atoms in Molecules*: *A Quantum Theory*; Oxford University Press: Oxford, U.K., 1990.

(35) Bader, R. F. W.; Johnson, S.; Tang, T.-H.; Popelier, P. L. A. *J. Phys. Chem.* **1996**, *100*, 15398.

(36) Becke, A. D.; Edgecombe, K. E. *J. Chem. Phys.* **1990**, *92*, 5397.

(37) Savin, A.; Nesper, R.; Wengert, S.; Fässler, T. *Angew. Chem., Int. Ed. Engl.* **1997**, *36*, 1808 and references therein.

(38) Zicovich-Wilson, C. M.; Dovesi, R.; Saunders: V. R. *J. Chem. Phys.* **2001**, *115*, 9708.

(39) Saunders: V. R.; Dovesi, R.; Roetti, C.; Orlando, R.; Zicovich-Wilson, C. M.; Harrison, N. M.; Doll, K.; Civalleri, B.; Bush, I. J.; D'Arco, Ph.; Llunell, M. *CRYSTAL03*; 2003, development version, available on web at http://www.crystal.unito.it.

(40) Lewis, J.; Schwarzenbach, D.; Flack, H. D. *Acta Crystallogr., Sect. A* **1982**, *38*, 733.

(41) Ching, W. Y.; Harmon, B. N. *Phys. Rev. B* **1986**, *34*, 5305.

(42) The CRYSTAL 98 web page, http://www.crystal.unito.it/Basis_Sets/ptable.html.

(43) Dovesi, R. Personal communication.

(44) Zicovich-Wilson, C. M.; Dovesi, R. Manuscript in preparation.

(45) Pipek, J.; Mezey, P. *J. Chem. Phys.* **1989**, *90*, 4916.